6

A novel catalyst for the electrochemical reduction of CO_2 to C_1-C_5 hydrocarbons

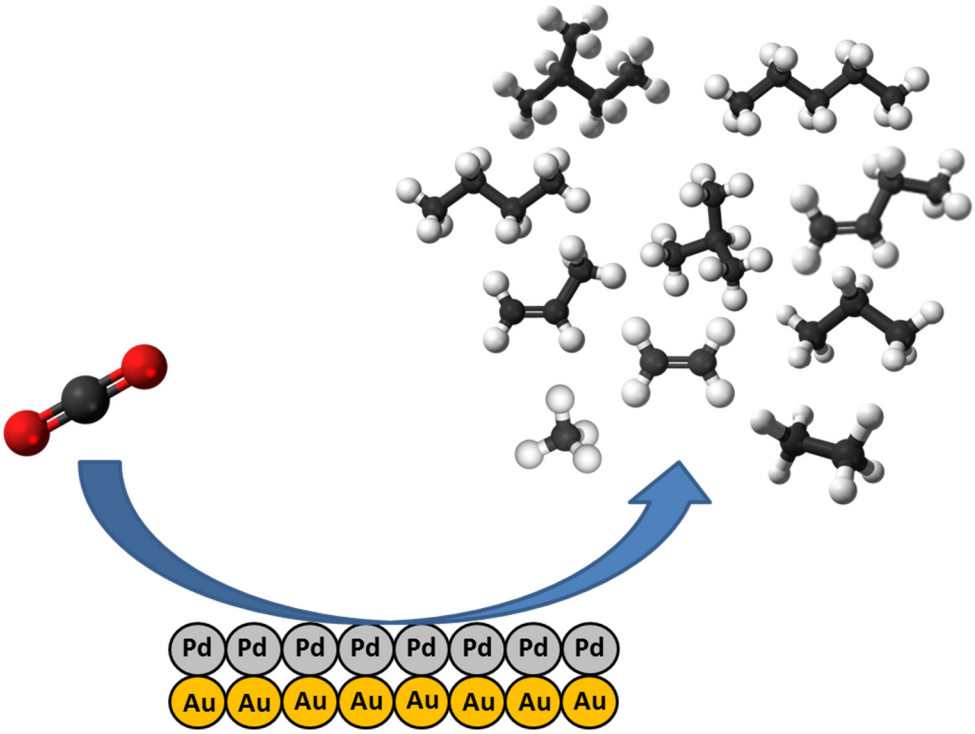

The contents of this chapter are being prepared for publication as: R. Kortlever, I. Peters, C. Balemans, R. Kas, Y. Kwon, G. Mul and M.T.M. Koper, *in preparation*.

Abstract The electrochemical reduction of CO_2 to valuable products, especially hydrocarbons, is a reaction of considerable interest to both scientists and society since it is a potential reaction for energy storage and conversion. Copper has been long known to be a unique catalyst for CO_2 reduction, since it is the only catalyst able to produce methane, ethylene and ethane from CO_2 with decent faradaic efficiencies. The special catalytic properties of copper have recently been related to its ability to bind and protonate CO, a key intermediate for the production of hydrocarbons, efficiently. Here we report on the design and synthesis of a new non-copper-containing catalyst that is able to reduce CO_2 to C_1 to C_5 hydrocarbons. This catalyst was designed by combining a metal that binds CO too strongly, palladium, with a metal that binds CO too weakly, gold, in an effort to tune the binding energy of CO on this catalyst. We show that a mixture of C_1-C_5 hydrocarbons is produced from an onset potential of -0.8 V vs. RHE. In addition to these hydrocarbons, soluble products such as formic acid, methanol, ethanol and acetic acid are observed. We propose that the higher hydrocarbons are formed via a polymerization of $–CH_2$ groups adsorbed on the catalyst surface.

6.1 Introduction

The electrocatalytic reduction of CO_2 to valuable products is a topic that has attracted the interest of many electrochemists and inorganic chemists recently. One of the main reasons for this increased interest is that the CO_2 reduction reaction is a potential reaction for energy storage and conversion. In a closed carbon cycle, CO_2 would be reduced to fuels using renewable energy while these fuels yield CO_2 once they are oxidized and thus release the stored energy. Thereby, a sustainable low-temperature redox cycle can be created that would decrease the potentially harmful emission of CO_2 into the atmosphere.

A major breakthrough in the electrochemical reduction of CO_2 was the discovery in 1985 by Hori et al. that copper is able to reduce CO_2 to hydrocarbons such as methane and ethylene with good faradaic efficiencies.[5] Since then ample research has been conducted to determine the special catalytic ability of copper for this reaction.[6-9] In early work, CO was found to be a key intermediate in the formation of hydrocarbons on copper[10,11] and recent calculations by Peterson et al. have indicated that a good catalyst for the reduction of CO_2 to methane should

catalyze the protonation of CO to HCO or COH efficiently.[12] If a catalyst binds CO too weakly, CO will desorb before this protonation can take place, while if a catalyst binds CO too strongly, significant overpotentials are required for this reduction step since the formation of HCO or COH is thermodynamically unfavorable.

Recently, Jaramillo et al. have shown that the production of hydrocarbons from CO_2 is not an unique ability of copper, since they detected small quantities of methane during CO_2 reduction on Ag, Zn, Ni, Pt and Fe.[13] Therefore, there is a strong indication that CO_2 reduction on metal electrocatalysts can be tuned to produce hydrocarbons, though limited to C_1 products. If we follow the theoretical findings of Peterson et al., the ability to make hydrocarbons from CO_2 can be influenced by tuning the binding energy of CO on the catalyst surface. In this Chapter we have therefore combined a metal which binds CO too weakly, in this case Au, with a metal which binds CO too strongly, namely Pd, in an effort to create an active electrocatalyst for the reduction of CO_2 to hydrocarbons which does not contain copper.

Pd-Au bimetallic catalysts have been studied in detail as both heterogeneous catalysts[14] and electrocatalysts,[15,16] and have recently also been employed as CO_2 reduction catalysts.[17,18] Plana et al. showed that the faradaic efficiency toward CO_2 reduction on Pd shell Au core nanoparticles increased with decreasing Pd shell thicknesses, since the faradaic efficiency toward hydrogen evolution decreased.[17] However, they did not show which products were formed using these catalysts. A recent study by Hahn et al. showed that formic acid was the dominant product of CO_2 reduction on thin PdAu alloy film synthesized by an electron-beam co-deposition method.[18] They observed that the alloy displays different catalytic properties toward CO_2 reduction than the parent metals, thereby further emphasizing that alloying can be an effective way to design new electrocatalysts for CO_2 reduction.

In this study the combination of Pd and Au was made by depositing both overlayers and monolayers of Pd on an Au substrate. We have studied the reduction of CO_2 on these materials both with electrochemical methods and with techniques that determine the products, both liquid and gaseous, online.

Remarkably we will show that both combinations of Pd and Au are able to produce C_1 to C_5 hydrocarbons. The onset potential for hydrocarbon production from CO_2 on these electrodes is -0.8 V vs. RHE, which is comparable to the onset potential for methane and ethylene production on copper electrodes. To the best of our knowledge, this is the first non-copper-containing electrocatalyst that produces such a variety of multi-carbon products form CO_2.

6.2 Experimental

6.2.1 Materials

Cylindrical polycrystalline gold and palladium electrodes (99.995% Au and 99.9% Pd, purchased at Mateck GmbH) with a diameter of 4.5 mm and 5 mm, respectively, embedded in Teflon were used as working electrodes in the standard electrochemical measurements. For faradaic efficiency measurements a polycrystalline gold plate (99.995% Au, Mateck GmbH) was used a working electrode. Prior to every experiment the working electrode was polished mechanically to a mirror-like finish using alumina pastes. Afterwards, the electrode was sonicated in ultra-pure water.

Electrolytes were made from ultra-pure water (Millipore MilliQ gradient A10 system, 18 mΩ cm) and high purity reagents (Sigma Aldrich TraceSelect). Before each experiment the electrolytes were first purged with Argon (Air Products, 5.7) for 15 minutes to remove air from the solution. In the case of CO_2 reduction experiments the electrolyte was subsequently purged with CO_2 (Linde, 4.5) for at least 30 minutes to saturate the solution.

6.2.2 Electrochemical Measurements

Cyclic voltammetry measurements were carried out in a standard electrochemical cell using a three-electrode assembly at room temperature. The cell and all other glassware were first cleaned by boiling in a 1:1 mixture of concentrated sulfuric

and nitric acid and were cleaned before every experiment by boiling in ultra-pure water. Either a gold electrode with a diameter of 4.5 mm or a palladium electrode with a diameter of 5 mm was used as working electrode. A coiled gold wire was used as counter electrode. All potentials are reported versus the reversible hydrogen electrode (RHE) as a reference electrode in a separate compartment filled with the same electrolyte, at the same pH as the electrolyte in the electrochemical cell. The voltammograms were recorded on an Ivium A06075 potentiostat at a scan rate of 50 mV s^{-1} unless stated otherwise.

Faradaic efficiency measurements were performed in a custom-made Teflon flow cell, consisting of two compartments separated with a Nafion 115 membrane. Both compartments had a volume of 12 ml which was filled with 10 ml electrolyte, leaving 2 ml gas headspace. Prior to use the flow cell was cleaned in a similar way as the cell used for cyclic voltammetry. A gold plate was used as a counter electrode, which was cleaned by flame annealing before experiments, and a Ag/AgCl reference electrode was used. All potentials were converted to the RHE scale using $V_{vs.\ RHE} = V_{vs.\ Ag/AgCl} + 0.197 + 0.059 \times 6.7$ (pH of the electrolyte). The resistance of the cell was determined before every experiment by electrochemical impedance spectroscopy (EIS) on an Ivium A06075 potentiostat. For the chronoamperometry measurements a Biologic VSP multichannel potentiostat was used, which compensated for 85% of the ohmic drop that was measured with EIS.

6.2.3 Electrode preparation

Palladium overlayers on a gold polycrystalline electrode (Pd-Au) were made by electrodepositing palladium onto gold from a 0.1 M H_2SO_4 + 1.0 mM $PdCl_2$ solution at 0.27 V vs. SCE for 60 seconds, using a procedure earlier used for the deposition of palladium on platinum.[19]

In order to deposit palladium monolayers, a monolayer of copper was first deposited on a polycrystalline gold electrode from a 0.1 M H_2SO_4 electrolyte containing 1 mM $CuSO_4$ using under potential deposition (UPD).[20] After determining the UPD region for copper on gold using cyclic voltammetry the polycrystalline gold electrode was held at -0.05 V vs. Ag/AgCl for 3 minutes, which

should correspond to a complete copper monolayer, after which the electrode was rinsed with ultra-pure water. The copper layer was subsequently displaced by palladium using of galvanic displacement. Therefore, the electrode was placed in a 0.1 M H_2SO_4 electrolyte containing 0.1 mM $PdCl_2$ at open circuit potential for 10 minutes.

6.2.4 Surface characterization

X-ray photoelectron spectroscopy (XPS) spectra were collected on a Quantera SXM (scanning XPS microprobe) spectrometer equipped with a monochromatic Al Kα x-ray source (1486.6 eV). The source was operated with a 25 W emission power, beam size of 200 µm and pass energy of 224 eV. The resolution of the spectrometer was 0.2eV and 0.8 eV for high resolution element scan and survey spectra, respectively.

Scanning electron microscopy (SEM) images were acquired using a FEI Nova NanoSEM 200 microscope.

6.2.5 Detection and Quantification of Products

For online detection of products dissolved in the electrolyte as a function of applied potential online High Performance Liquid Chromatography (HPLC) was used.[21] While changing the potential from 0.0 V to the required potential, samples were collected with an open tip positioned close (~10 µm) to the electrode. Sampling was done at a rate of 60 µL min^{-1} and each sample had a volume of 60 µL. Since the potential was changed at 1 mV s^{-1}, each sample contained the products averaged over a potential change of 60 mV. After voltammetry, these samples were analyzed by HPLC (Prominence HPLC, Shimadzu; Aminex HPX 87-H column, Biorad).

Online Electrochemical Mass Spectrometry (OLEMS) was used to detect gaseous products of the reactions.[22] The products were collected with a small hydrophobic tip which was positioned close (about 10 µm) to the electrode with

the aid of a camera. The tip was constructed as a porous Teflon cylinder with a diameter of 0.5 mm and an average pore size of 10-14 µm in a Kel-F holder. The tip is connected to a mass spectrometer with a PEEK capillary. Before use the tip was cleaned in a solution of 0.2 M $K_2Cr_2O_7$ in 2 M H_2SO_4 and rinsed thoroughly with Millipore water. A secondary electron multiplier (SEM) voltage of 2400 V was used for detection in a Balzers Quadrupole mass spectrometer, except for hydrogen (m/z = 2) where a SEM voltage of 1200 V was used. The products were measured while changing the potential of the electrode from 0.0 V to -1.5 V, and back at 1 mV s^{-1}.

Quantitative faradaic efficiency measurements of the gas products were carried out using Gas Chromatography (GC).[23,24] At atmospheric pressure, CO_2 was continuously purged through a two-compartment flow cell at a rate of 5 mL/min for 20 min to saturate the electrolyte. The flow rate was decreased to 2 mL/min while a constant potential was applied for 30 minutes. The cell effluent was sampled via GC once every 6 minutes. CO, CO_2, H_2 and hydrocarbons were simultaneously separated using two series columns (ShinCarbon 2 m micropacked column and Rtx-1). The quantitative analysis of the gas products was performed using a thermal conductivity detector (TCD) and flame ionization detector (FID).

Liquid products formed during electrolysis were identified with 1D and 2D ^{1}H-NMR. First, an electrolysis experiment was conducted using the same two-compartment flow cell used for the GC experiment. A potential of -1.2 V vs. RHE, corrected for the resistance of the cell, was applied for 15 hours. Afterwards, samples were taken from the catholyte and prepared for NMR analysis by addition of D_2O (sample to D_2O ratio = 9:1). The NMR experiments were perfomed on a Bruker AV-III 600 MHz NMR spectrometer, using a presaturation sequence to suppress the water signal.

6.3 Results and discussion

6.3.1 CO_2 reduction on palladium and gold electrodes

Palladium and gold have both already been studied extensively as electrocatalysts for the electrochemical reduction of CO_2.[1,25-28] Both palladium and gold have been shown to form CO as main products, with gold being more selective towards CO with tiny fractions of hydrocarbons as side-products. Palladium has been reported to form small amounts of methane,[1,26] while one report showed the production small fractions (≤ 1%) of C_1-C_3 hydrocarbons on gold.[27] The production of hydrocarbons is however generally not shown for gold electrodes.[13,29] However, in order to create a frame of reference we will start by discussing the reduction of CO_2 on both materials as studied with the techniques that will be employed later on in this article to evaluate CO_2 reduction on palladium-gold bimetallic catalysts.

The reduction of CO_2 on palladium and gold polycrystalline electrodes in a pH 6.7 phosphate buffer was studied with voltammetry as well as with OLEMS and online HPLC, in order to gain insight in the production of both liquid and gaseous products from CO_2 as a function of potential. Cyclic voltammograms of a palladium electrode in a pH 6.7 phosphate buffer purged with argon, as blank, showed a higher current density than voltammograms in the same electrolyte purged with CO_2 (see Figure 6.1b). This is to be expected since palladium is a good catalyst for the hydrogen evolution reaction (HER) that occurs in the same potential window as CO_2 reduction.[30,31] CO_2 reduction is expected to take place at the same catalytic sites as hydrogen evolution and thus will block the hydrogen evolution reaction. Since the rate of hydrogen evolution is faster than the rate of CO_2 reduction the current density decreases when CO_2 is introduced in the system. Cyclic voltammograms with a gold electrode in a pH 6.7 phosphate buffer show the opposite trend since gold is a poor catalyst for the HER, but is active for CO_2 reduction (see Figure 6.1a).[1,31]

The production of methane (m/z = 15) and small amounts of ethylene (m/z = 26) from CO_2 on a polycrystalline palladium electrode was observed starting at an onset potential of -1.0 V vs. RHE (see Figure AIII.2). However, it

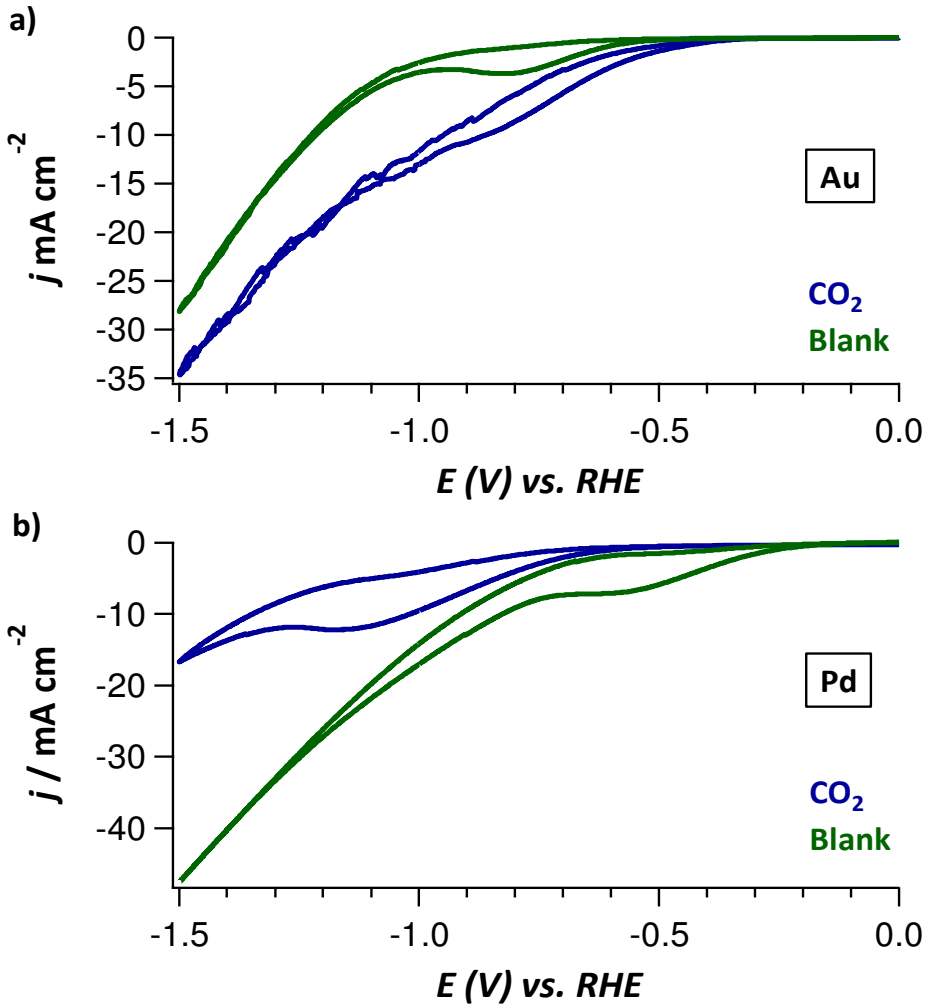

Figure 6.1 a) Cyclic voltammograms of a polycrystalline gold electrode recorded in a 0.1 M KH_2PO_4 / 0.1 M K_2HPO_4 electrolyte (pH 6.7) at a scan rate of 50 mV/s purged with either argon (green) or CO_2 (blue); **b)** Cyclic voltammograms of a polycrystalline palladium electrode recorded in a 0.1 M KH_2PO_4 / 0.1 M K_2HPO_4 electrolyte (pH 6.7) at a scan rate of 50 mV/s purged with either argon (green) or CO_2 (blue).

should be noted that with the OLEMS setup we were unable to measure CO production, since CO_2 fragments into CO in the ion chamber of the mass spectrometer forming CO. Therefore, it is impossible to accurately determine the production of CO, though we do assume that CO is formed at the palladium electrode as has been reported previously.[28,32] Formic acid was detected as liquid product from CO_2 reduction on palladium starting at an onset potential of -1.2 V vs. RHE (see Figure AIII.7). The reduction of CO_2 on a polycrystalline gold electrode did not yield any liquid products and no production of hydrocarbons was detected during OLEMS measurements (see Figure AIII.3). As is well known, CO is the main product of CO_2 reduction on gold.[1,29]

6.3.2 CO_2 reduction on palladium overlayers on a gold substrate

The structure of the electrodeposited layers of palladium on gold was visualized with scanning electron microscopy (SEM), showing that palladium completely covers the gold substrate (see Figure AIII.1). As was the case with palladium electrodepostion on platinum, some holes in the deposition layers can be seen, but since the concentration of these defects is low we do not expect them to play a major role in the catalytic properties of the material. Two palladium structures are seen in the deposition layer; the first is a scale-like structure, while the second is a triangular structure suggesting a preferential (111) configuration, similar to palladium deposited on platinum. Since the palladium deposition layer shows a roughened nanostructured surface, it is very difficult to exactly determine the deposition layer thickness, since this will vary along the electrode surface. From the coulombic charge of palladium deposition, which was typically around 4.5 mC, an average thickness of 65-75 monolayers of palladium was estimated. Copper UPD measurements showed an increase in surface area of 1.18 times compared to a palladium polycrystalline electrode.

An electrochemical characterization of the Pd-Au electrode in 0.5 M H_2SO_4 was performed (see Figure 6.2a). Both palladium-like as gold-like behavior is observed in the voltammogram, since hydrogen adsorption and desorption is seen as well as an (surface) oxide reduction peak around 0.7 V vs. RHE which is to

be expected for the reduction of a palladium-rich oxide region, in combination with an (surface) oxide reduction peak around 1.2 V vs. RHE which is to be expected for the reduction of a gold-rich oxide region.[16]

The presence of both palladium and gold near the surface is confirmed by XPS spectra of the Pd-Au electrodes (see Figure AIII.15-17). The presence of palladium was confirmed from the Pd 3*d* spectra, which showed two separated peaks at 340.7 eV and 335.4 eV, corresponding to the $3d_{3/2}$ and $3d_{5/2}$ of metallic palladium. These values show a slight shift to higher binding energies compared to literature data that report the $3d_{3/2}$ peak at 340.4 eV and the $3d_{5/2}$ peak at 335.1 eV.[33,34] Small peaks were observed in the Au 4*f* spectral region, with an overlap of Pd 4*s*. Both the peaks for Au $4f_{5/2}$ and $4f_{7/2}$ showed no shift compared to a blank measurement with the gold substrate. Since the peaks for gold were significantly smaller than the palladium peaks, the atomic percentage of palladium on or near the surface is higher than gold.

Cyclic voltammograms of a Pd-Au electrode in a pH 6.7 phosphate buffer purged with either argon or CO_2, shown in Figure 6.2b, show a high degree of similarity with the cyclic voltammograms measured with a palladium electrode (Figure 6.1b). A reduction peak around -0.2 V vs. RHE was seen in the first scan (see Figure 6.2c), which was not present in the later scans. At Pd-Pt a similar peak was observed around -0.4 V vs. RHE. Comparing our voltammograms with the reported voltammograms for CO_2 reduction on PdAu core-shell nanoparticles with different shell thicknesses, we do not observe any pre-peaks around -0.5 V vs. RHE.[17] The reduction of CO_2 starts around -0.6 V vs. RHE and a plateau is seen around -1.1 – -1.2 V vs. RHE as is also seen with polycrystalline palladium.

Formic acid was observed as the dominant soluble product from CO_2 reduction on Pd-Au with online HPLC (see Figure 6.3). The production of formic acid on Pd-Au shows many similarities to the production of formic acid on Pd-Pt.[19] In both cases a low overpotential peak in the production of formic acid is seen, which is correlated with the reduction peak around -0.2 V vs. RHE in the voltammetry, followed by a continuous production of formic acid at higher overpotentials (≤ -1.0 V vs. RHE). In the case of Pd-Pt the low overpotential production of formic acid was the result of (in-)direct bicarbonate reduction to

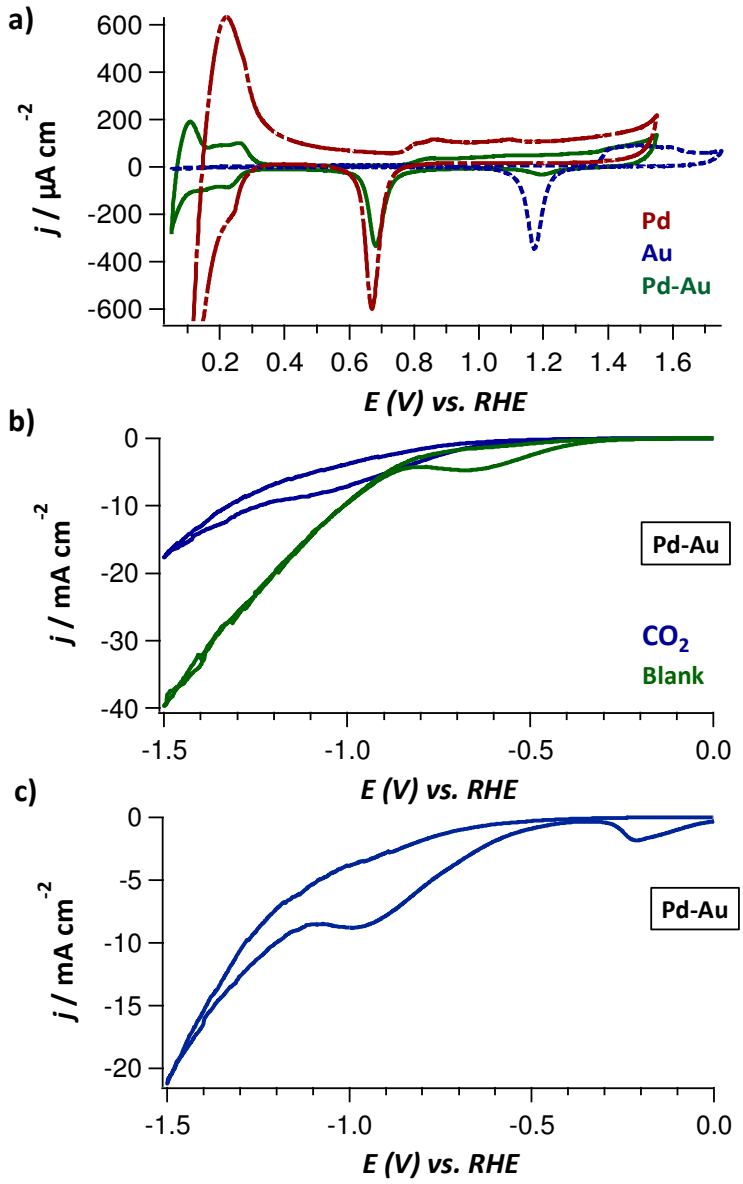

Figure 6.2. a) Cyclic voltammograms of a palladium electrode (red dashed line), gold electrode (blue dashed line) and a Pd-Au electrode (green solid line) in a 0.5 M H_2SO_4 electrolyte purged with argon at a scan rate of 20 mV/s; **b)** Cyclic voltammograms of a Pd-Au electrode recorded in a 0.1 M KH_2PO_4 / 0.1 M K_2HPO_4 electrolyte (pH 6.7) at a scan rate of 50 mV/s purged with either argon (green) or CO_2 (blue); **c)** First voltammogram of a Pd-Au electrode in a CO_2 saturated 0.1 M KH_2PO_4 / 0.1 M K_2HPO_4 electrolyte (pH 6.7).

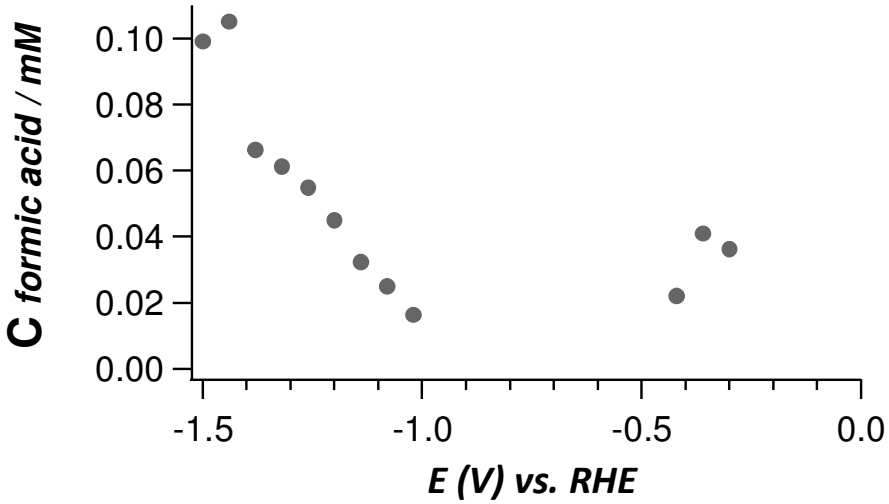

Figure 6.3. Formation of formic acid during CO_2 reduction on a Pd-Au electrode followed with online HPLC in a pH 6.7 phosphate buffer electrolyte (0.1 M KH_2PO_4/ 0.1 M K_2HPO_4).

formic acid, while the high overpotential production of formic acid was due to the reduction of CO_2 to formic acid.[19] Considering the large similarities between the production of formic acid on both catalysts, the same explanation is assumed to be valid for Pd-Au. This assumption is further supported by a recent observation that gold is also able to (in-)directly reduce bicarbonate to formic acid.[35]

Formic acid was however not the only dissolved product detected after 15 hours of electrolysis at -1.2 V vs. RHE (the potential at which a reduction plateau is observed in the voltammetry). ^{1}H-NMR shows the production of methanol, ethanol and acetic acid (see Table AIII.1 and Figure AIII.8). The peak for methanol was substantially lower than the peak for formic acid, indicating that the concentration of methanol is also substantially lower than the concentration of formic acid. Since the detection limit for methanol with our HPLC system is also higher than the detection limit for formic acid, both of these facts explain why methanol was not observed with online HPLC. Ethanol showed very small peaks in the ^{1}H-NMR spectrum and its identity was confirmed by the coupling of the -CH_3 and -CH_2 peaks of ethanol in 2D homonuclear COSY (see Figure AIII.9).

Furthermore, a small peak indicating the presence of acetic acid was observed. Some other peaks were also present in the ^{1}H-NMR spectrum at low chemical shifts, however these proved to be small impurities in the electrolyte and not products that were formed during electrolysis.

The reduction of CO_2 on Pd-Au studied with OLEMS shows the production of hydrocarbons (see Figure 6.4). Both methane (m/z = 15) and ethylene (m/z = 26) were observed starting from -0.8 V vs. RHE and, interestingly, higher mass fractions pointing to the production of C_3 hydrocarbons (m/z = 39, m/z = 42 and m/z = 43), either propane or propylene, and the production of C_4 hydrocarbons (m/z = 56 and m/z = 58), either butane or butene, were detected. Since no major soluble products other than formic acid were detected, the detection of these higher mass fractions cannot be related to the production of higher aldehydes or alcohols. Figure 6.4 thus provides convincing evidence that Pd-Au is able to produce C_1 to C_4 hydrocarbons from CO_2. All of these hydrocarbons are produced starting from an onset potential of -0.8 V vs. RHE, and the intensity of the detected hydrocarbons decreases from C_1 to C_4. Furthermore, all hydrocarbon mass fragments show a decrease at potentials close to -1.5 V vs. RHE suggesting that the optimal potential for the production of hydrocarbons on this material lies between -1.1 V vs. RHE and -1.4 V vs. RHE.

The onset potential of -0.8 V vs. RHE for the reduction of CO_2 to hydrocarbons on Pd-Au is 400 mV less negative than the onset potential for the production of methane and ethylene that was observed for a polycrystalline palladium electrode. Also, this onset potential is very comparable with the onset potential of CO_2 reduction to hydrocarbons on copper in the same electrolyte, which is -0.6 V vs. RHE for ethylene and -0.8 V vs. RHE for methane.[7] Recently, Jaramillo et al. showed the production of methane and methanol on transition metals like Au, Ag, Pt, Zn, Ni and Fe, however this study did not show the production of higher hydrocarbons.[13] Furthermore, the reduction of CO_2 on copper-containing catalysts is generally reported to produce only methane, ethylene and ethane as hydrocarbon products, with the exception of one study reporting the production of higher hydrocarbons on polycrystalline copper,[36] and a recent study showing the production of C_1-C_4 hydrocarbons on a Cl-induced biphasic Cu_2O-Cu catalyst.[37] The production of ethanol, n-propanol and allyl alcohol as intermediate products

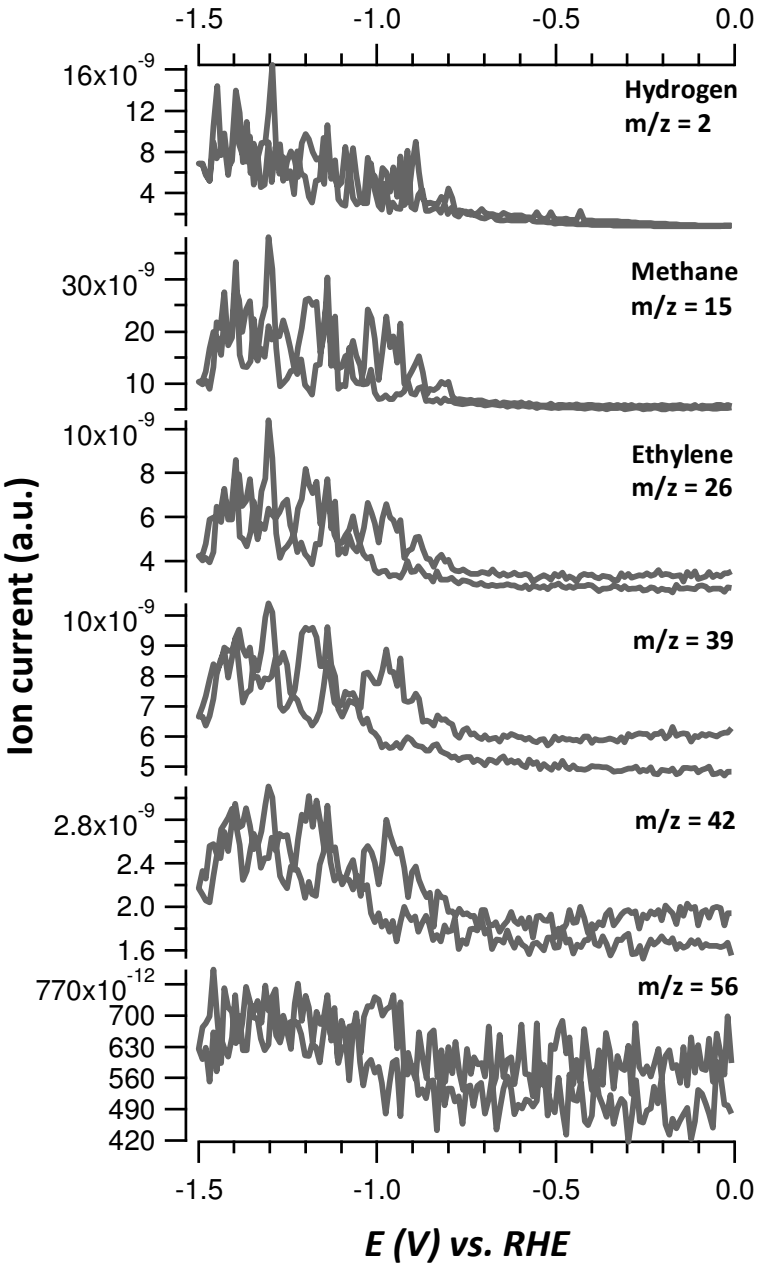

Figure 6.4 Formation of hydrogen (m/z = 2), methane (m/z = 15) ethylene (m/z = 26), C_3 hydrocarbons (m/z = 39 and 42) and C_4 hydrocarbons (m/z = 56) from CO reduction on a Pd-Au electrode followed with OLEMS in a pH 6.7 phosphate buffer electrolyte (0.1 M KH_2PO_4/ 0.1 M K_2HPO_4).

and multiple C_2 and C_3 trace products have been reported as soluble products for CO_2 reduction on copper.[1,9]

To study changes in the surface composition of the electrodes during the production of hydrocarbons, XPS spectra of the Pd-Au electrodes were obtained after 30 minutes of electrolysis at -1.2 V vs. RHE (see Figure AIII.18-20). Both gold and palladium were still observed and a small shift was seen in the Pd $3d_{3/2}$ and $3d_{5/2}$ peaks to higher binding energies, 341.0 eV and 335.7 eV respectively.

It is known that CO is a key intermediate in the formation of hydrocarbons from the reduction of CO_2 on copper.[10,11] To confirm that CO is also a key intermediate in the production of hydrocarbons on Pd-Au, the reduction of CO on Pd-Au was studied using OLEMS (see Figure 6.5). All mass fragments that were previously observed for CO_2 reduction are also detected when CO reduction is performed. This proves that, as is the case for copper catalysts, CO is the main intermediate by which hydrocarbons are formed on the Pd-Au catalyst. The onset potentials for the production of hydrocarbons have however shifted slightly for CO reduction in comparison with CO_2 reduction. The onset potential for the reduction of CO to hydrocarbons lies between -0.6 V – -0.7 V vs. RHE while the onset potential for CO_2 reduction to hydrocarbons lies around -0.8 V vs. RHE. Interestingly, the onset potential for CO reduction to hydrocarbons coincides with the onset potential of HER, implying that the hydrogenation of CO could be the potential determining step in the production of hydrocarbons from CO. CO_2 reduction to hydrocarbons starts at potentials at which HER is already taking place, indicating that the reduction of CO_2 to CO would be the potential determining step for this process.

To determine the faradaic efficiencies toward the production of the hydrocarbons and CO on Pd-Au and to further elucidate the identity of the hydrocarbon products, chronoamperometry experiments with a custom-made flow cell with a high exposed cathode surface area and a low electrolyte volume were performed. The effluent stream of gasses coming from the flow cell was analyzed using gas chromatography.

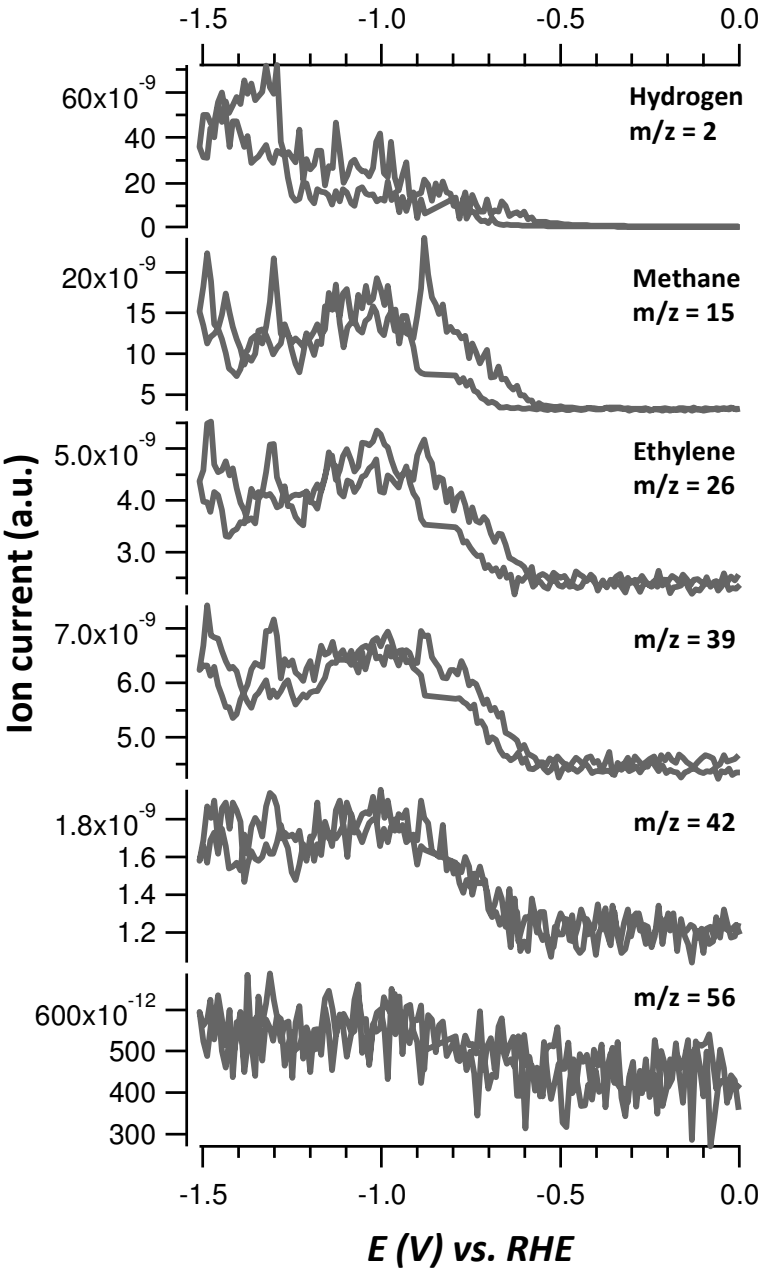

Figure 6.5 Formation of hydrogen (m/z = 2), methane (m/z = 15) ethylene (m/z = 26), C_3 hydrocarbons (m/z = 39 and 42) and C_4 hydrocarbons (m/z = 56) from CO reduction on a Pd-Au electrode followed with OLEMS in a pH 6.7 phosphate buffer electrolyte (0.1 M KH_2PO_4/ 0.1 M K_2HPO_4).

At all the studied potentials the production of CO was observed (see Figure 6.6a). The production of CO reached a peak at -0.6 V vs. RHE, with a maximum faradaic efficiency of 30.9%. Such a faradaic efficiency is higher than faradaic efficiencies measured on Pd wires[32] but significantly lower than the faradaic efficiency for CO production on Pd nanoparticles[38] and on Au nanoparticles.[29] At -0.8 V vs. RHE and potentials more negative the production of hydrocarbons was observed, in agreement with the onset potential detected with OLEMS. The dominant hydrocarbon that was produced was methane, reaching a maximum faradaic efficiency of 2% at -1.4 V vs. RHE (see Figure 6.6b). Both ethylene and ethane are produced as C_2 hydrocarbons, with a higher faradaic efficiency toward ethane compared to ethylene. The superior faradaic efficiencies toward ethane are believed to be due to high amounts of hydrogen that is produced at the PdAu electrode. The electrode will therefore be able to convert

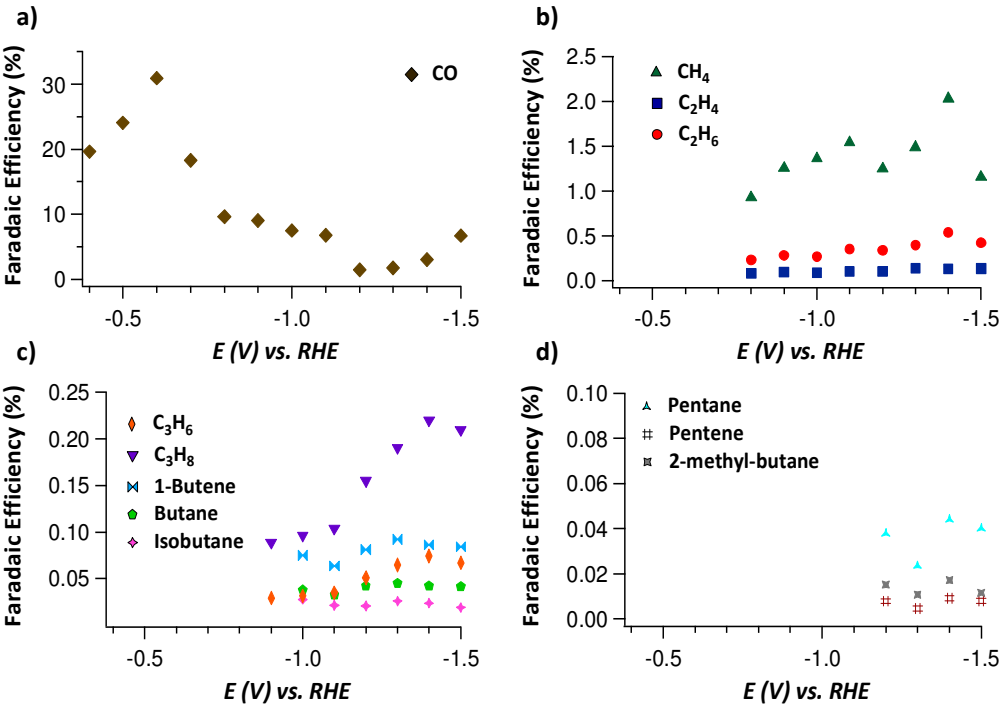

Figure 6.6 Faradaic efficiencies for the reduction of CO_2 on Pd-Au in a pH 6.7 phosphate buffer electrolyte (0.1 M KH_2PO_4/ 0.1 M K_2HPO_4) toward different C_1-C_5 hydrocarbon products.

unsaturated hydrocarbons to saturated hydrocarbons. A maximum faradaic efficiency of 0.7 % toward C_2 hydrocarbons is achieved at -1.4 V vs. RHE.

At -0.9 V vs. RHE and more negative potentials the production of propane and propylene as C_3 hydrocarbons and butane, 1-butene and isobutene as C_4 hydrocarbons is detected, as shown in Figure 6.6c. The production of propane shows higher faradaic efficiencies than the production of propylene, as was the case with the C_2 hydrocarbons. The total faradaic efficiency toward C_3 hydrocarbons reaches a maximum of approximately 0.3% at -1.4 V vs. RHE. A mixture of butane, 1-butene and isobutene was detected as C_4 hydrocarbons. Here 1-butene was the dominant species, indicating that the hydrogenation of the hydrogenation of 1-butene is less favorable than the hydrogenation of ethylene and propylene. The amount of C_4 hydrocarbons is small, as was already shown with OLEMS, constituting to only 0.16% faradaic efficiency at -1.3 V vs. RHE.

Next to the previously mentioned hydrocarbons, small amounts of C_5 hydrocarbons were detected at -1.2 V vs. RHE and lower potentials. Out of the C_5 hydrocarbons pentane was produced dominantly, followed by 2-methyl-butane and pentene, respectively. The highest faradaic efficiency toward C_5 hydrocarbons, 0.07%, was achieved at -1.4 V vs. RHE.

The production of C_3 and higher hydrocarbons on PdAu electrodes may go through different mechanistic pathways than the production of hydrocarbons on Cu electrodes, since Cu generally only produces C_1 and C_2 hydrocarbons.[4,7] We propose that the production of these higher hydrocarbons on PdAu proceeds via a coupling of -CH_2 groups that are adsorbed on the electrode, as is the case for the production of ethylene on Cu at higher applied overpotentials,[4,39,40] or via CO insertion in a Fischer-Tropsch-like step. This also explains the production of branched hydrocarbons such as isobutane and 2-methyl-butane. Since such an coupling mechanism is essentially a polymerization of absorbed -CH_2 groups, it should give a hydrocarbon product distribution that obeys the Flory-Schulz distribution. The chain growth probability is commonly given as a function of the weight fractions of the products as is expressed in equation 1:[36,41]

$$w_n = (\ln^2 a) \cdot n a^n \qquad (1)$$

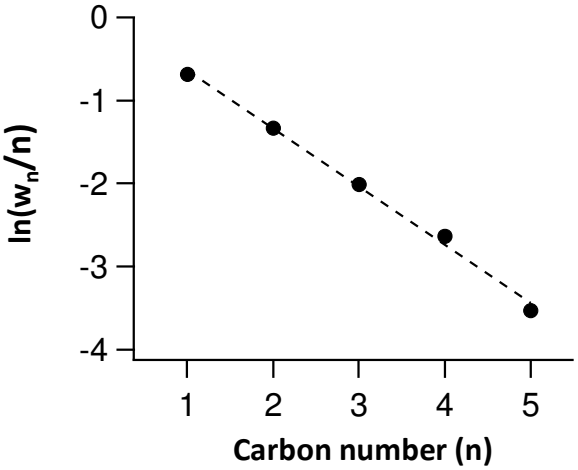

Figure 6.7 Flory-Schulz product distribution of the hydrocarbon products produced at -1.5 V vs. RHE on a Pd-Au electrode in a pH pH 6.7 phosphate buffer electrolyte (0.1 M KH_2PO_4/ 0.1 M K_2HPO_4). w_n : weight fraction, n : carbon number.

in which w_n is the weight fractions of the product, with carbon number n and *α* is the chain growth probability. In Figure 6.7 a Flory-Schulz distribution is plotted for the total amounts of C_1-C_5 hydrocarbons produced at -1.5 V vs. RHE. A clear linear correlation is seen for the produced hydrocarbons, providing additional support for the hypothesis that these hydrocarbons are produced by the coupling of -CH_2 groups.

6.3.3 CO_2 reduction on palladium monolayers on a gold substrate

To obtain more insight into the effect of palladium coverage, palladium monolayers (MLs) were deposited on a gold polycrystalline electrode via galvanic displacement of a copper UPD layer and were employed for the reduction of CO_2. It should be noted that the reported monolayers do not necessarily have to be complete monolayers of palladium covering gold, since the most important issue for this study was finding a means to control the amount of palladium on the gold electrode. Electrochemical characterization of the deposited monolayers in a 0.5 M H_2SO_4 electrolyte showed a current increase in the hydrogen UPD region with an increasing palladium layer thickness of 1 ML to 4 MLs, therefore confirming the

higher amount of palladium on the electrode (see Figure AIII.11). "1 ML" of Pd should therefore be considered as the amount necessary for the replacement of 1 Cu UPD layer.

Both gold and palladium were observed in XPS spectra of a gold electrode covered with 4 MLs of Pd (see Figure AIII.21-24). Besides gold and palladium, a copper contamination was observed indicating that not all the copper was replaced by galvanic displacement with palladium. The Pd 3*d* spectra showed peaks at 340.3 eV for $3d_{3/2}$ and 335.1 eV for $3d_{5/2}$. Compared to the Pd-Au electrode these peaks have thus shifted to lower binding energies, with the peak for $3d_{3/2}$ shifting to a slightly lower binding energy than bulk palladium which has been reported before for palladium monolayers on Au(111).[42]

A voltammetric study of CO_2 reduction on the palladium MLs on gold showed similar responses for all the different palladium layer thicknesses (see Figure AIII.12). In all cases, a decrease in current was observed when CO_2 was present in the electrolyte compared to blank scans with argon, indicating that the electrodes interact strongly with CO_2. The overall current profiles however were very similar and also very comparable to the voltammetry of palladium overlayers on gold as was discussed earlier.

The production of formic acid as detected with online HPLC on 1 ML of palladium on gold is more irregular than with 2-4 MLs of palladium on gold (see Figure 6.8). This can be caused by the a difference in production of gas bubbles near the electrode which can interfere with the sample collection of the online HPLC. A clear trend is observed in the production of formic acid with varying palladium layer thickness: The low overpotential production of formic acid is constant with the exception of a slight increase in formic acid production with 4 palladium monolayers, while the high overpotential production of formic acid increases with an increase in the number of palladium layers. Furthermore, with an increase in palladium on the electrode there is an increase in separation between the low overpotential production of formic acid and the high potential production of formic acid, meaning that no formic acid is produced in the intermediate potentials.

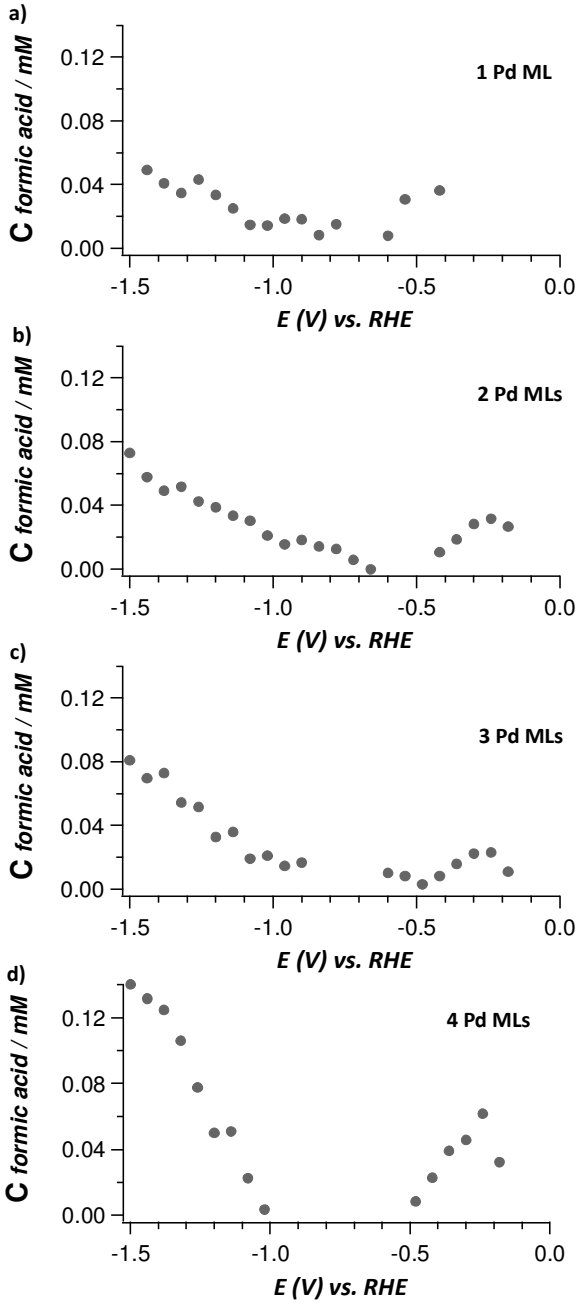

Figure 6.8 Formation of formic acid from CO reduction on a polycrystalline gold electrode covered with 1-4 MLs palladium monolayers (a-d) followed with online HPLC in a pH 6.7 phosphate buffer electrolyte (0.1 M KH_2PO_4/ 0.1 M K_2HPO_4).

Using OLEMS, a difference was observed in hydrocarbon distribution for different palladium layer thicknesses (see Figure 6.9 and Figures AIII.4-6). For 1 ML of palladium on gold only the production of C_1 to C_3 hydrocarbons from CO_2 is observed, while with 2 and 3 MLs of palladium a small amount of C_4 species is seen and with 4 MLs a clear rise is seen in C_4 species (m/z = 56). In general, higher intensities of higher hydrocarbon mass fragments are seen with increasing palladium layer thicknesses, indicating that a high ratio of palladium in comparison with gold on the surface is beneficial for the reduction of CO_2 to hydrocarbons on this catalyst.

To compare the production of hydrocarbons on Pd-Au and palladium monolayers on gold, the faradaic efficiency toward the reduction of CO_2 to CO and hydrocarbons on a gold polycrystalline electrode covered with 4 monolayers of palladium was studied (see Figure 6.10). The faradaic efficiency of CO_2 reduction to CO in this system is considerably higher than for Pd-Au, reaching a peak of 81.4 % at -0.5 V vs. RHE compared to the peak of 30.9 % at -0.6 V vs. RHE for Pd-Au. This catalytic behavior is to be expected since the amount of gold near or on the surface during CO_2 reduction will be higher for the palladium monolayer catalyst than for Pd-Au electrodes. Therefore this catalyst will display more gold-like properties, including a high efficiency toward CO production. This could also be beneficial for the production of hydrocarbons on this catalysts since in section 6.3.2 it was shown that CO is the main intermediate for the production of hydrocarbons on Pd-Au.

An additional benefit of a more gold-like catalytic behavior is also that the catalyst will be less prone to evolve hydrogen, boosting the efficiencies for CO_2 reduction. This is reflected in the observed faradaic efficiencies toward hydrocarbons. A maximum efficiency of 4.5% for methane production, 0.4% for ethylene production and 1.2% for ethane production is seen at -0.8 V vs. RHE, which decreases with more negative applied potentials. Compared to the Pd-Au electrode this is a two-fold increase in efficiency toward these hydrocarbons. The decrease in faradaic efficiency of hydrocarbon production with more negative potentials is assumed to be related with an increase in hydrogen production.

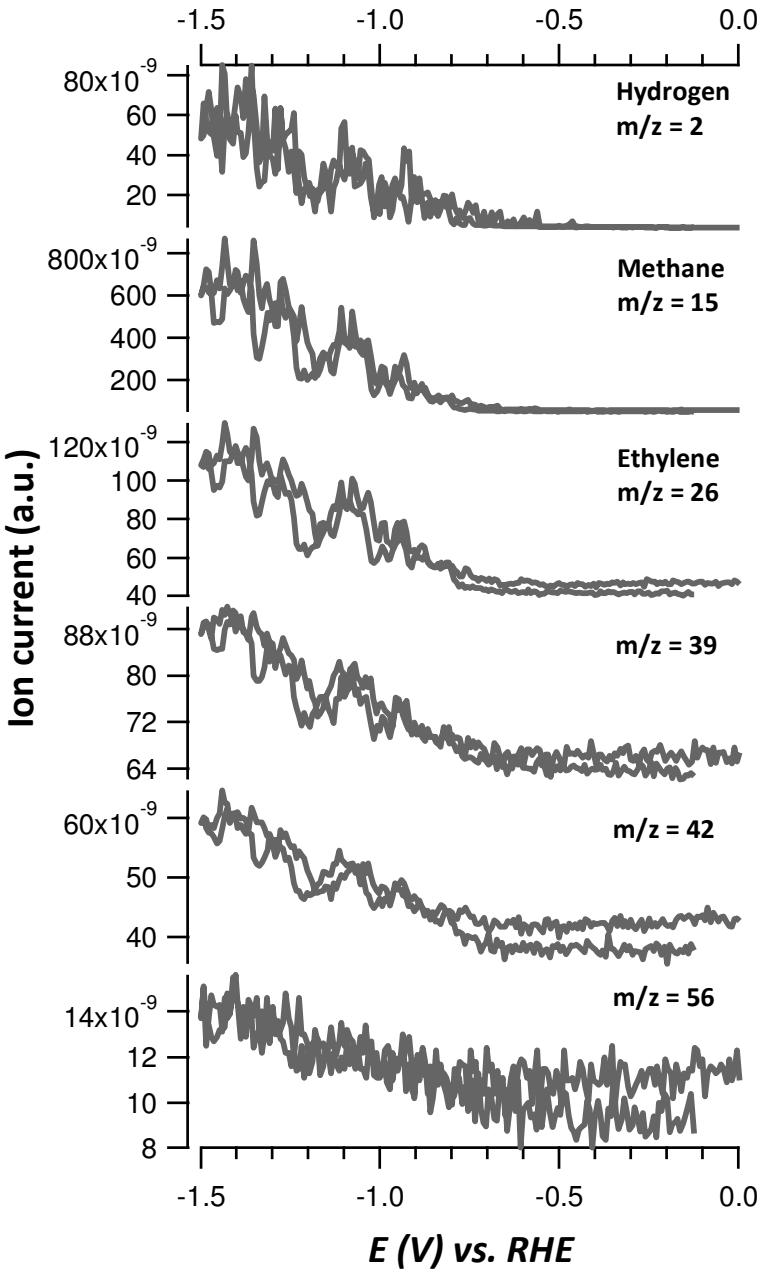

Figure 6.9 Formation of hydrogen (m/z = 2), methane (m/z = 15) ethylene (m/z = 26), C_3 hydrocarbons (m/z = 39 and 42) and C_4 hydrocarbons (m/z = 56) from CO_2 reduction on a polycrystalline gold electrode covered with 4 MLs palladium followed with OLEMS in a pH 6.7 phosphate buffer electrolyte (0.1 M KH_2PO_4/ 0.1 M K_2HPO_4).

The production of C_3 and C_4 hydrocarbons is observed starting from -1.0 V vs. RHE. Also for these products an increase in faradaic efficiency was seen in comparison with Pd-Au. The maximum faradaic efficiency toward C_3 hydrocarbons was 0.45% at -1.1 V vs. RHE, while the maximum faradaic efficiency toward C_4 hydrocarbons was 0.22% at -1.1 V vs. RHE.

At -1.1 V vs. RHE the production of C_5 hydrocarbons is observed. This onset potential is 100 mV less negative than the onset potential on Pd-Au, which is a consequence of easier detection since the concentrations of C_5 products that are produced are higher than on Pd-Au. The faradaic efficiencies toward C_5 products are higher than on Pd-Au, reaching a maximum of 0.11% at -1.1 V vs. RHE.

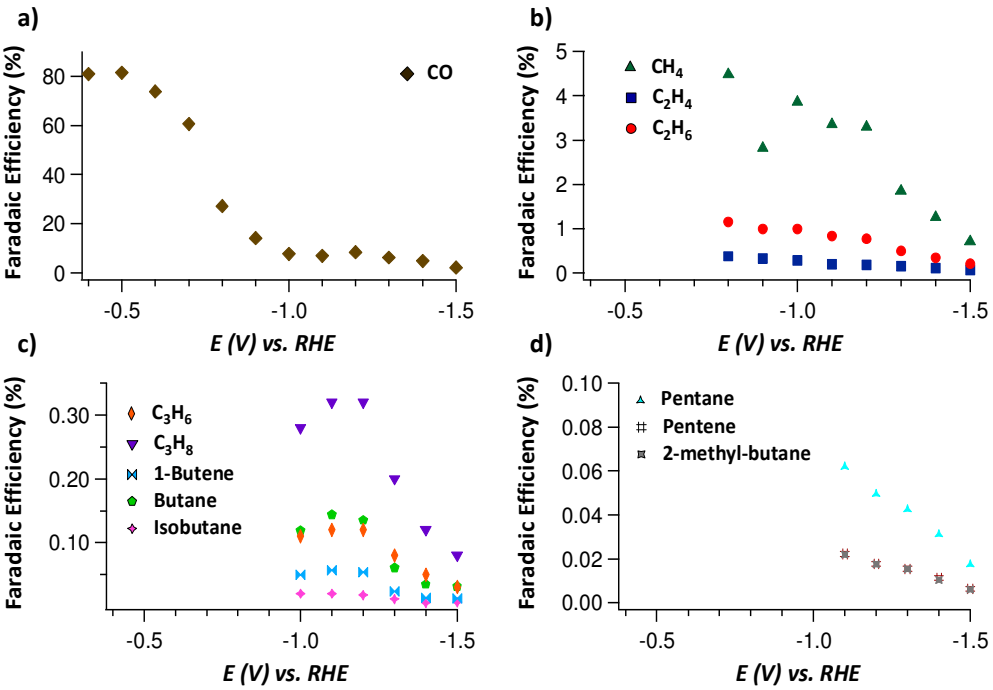

Figure 6.10 Faradaic efficiencies for the reduction of CO_2 on an Au electrode covered with 4 Pd MLs in a pH 6.7 phosphate buffer electrolyte (0.1 M KH_2PO_4/ 0.1 M K_2HPO_4) toward different C_1-C_5 hydrocarbon products.

6.4 Conclusions

We have shown that by combining a metal which binds CO too strongly and a metal which binds CO too weakly, the activity toward the production of hydrocarbons from CO_2 reduction can be tuned. By combining Au and Pd we obtain a mixture of C_1 to C_5 hydrocarbons, consisting of methane, ethylene, ethane, propylene, propane, 1-butene, isobutane, butane, 2-methyl-butane, pentane and pentene, and soluble products such as formic acid, methanol, ethanol and acetic acid. We propose that the higher hydrocarbons are produced by a polymerization of $-CH_2$ intermediates adsorbed on the surface. The production of hydrocarbons from CO_2 starts at an onset potential of -0.8 V vs. RHE, while the reduction of CO to hydrocarbons starts at a slightly lower onset potential of -0.6 V vs. RHE. This is an indication that CO is a key intermediate in the production of hydrocarbons on PdAu and that the reduction of CO_2 to the CO intermediate is the potential determining step. Furthermore, we show that by increasing the amount of Pd on a polycrystalline Au electrode, the activity toward hydrocarbon production increases. This is a strong indication that the active catalyst for the production of hydrocarbons is a Pd rich PdAu alloy near or on the surface.

References

(1) Y. Hori in *Modern Aspects of Electrochemistry*; Vayenas, C.; White, R.E.; Gamboa-Aldeco M.E. Eds.; Springer: New York, 2008; Vol. *42*, pp. 89-189.

(2) Rakowski DuBois, M.; DuBois, D.L. *Acc. Chem. Res.* **2009**, *42*, 1974.

(3) Sánchez-Sánchez, C. M.; Montiel, V.; Tryk, D. A.; Aldaz, A.; Fujishima, A. *Pure Appl. Chem.* **2001**, *73*, 1917.

(4) Kortlever, R.; Shen, J.; Schouten, K. J. P.; Calle-Vallejo, F.; Koper, M. T. M. *J. Phys. Chem. Lett.* **2015**, *6*, 4073.

(5) Hori, Y.; Kikuchi, K.; Suzuki, S. *Chem. Lett.* **1985**, *11*, 1695.

(6) Gattrell, M.; Gupta, N.; Co, A. *J. Electroanal. Chem.* **2006**, *594*, 1.

(7) Schouten, K. J. P.; Kwon, Y.; van der Ham, C. J. M.; Qin, Z.; Koper, M. T. M. *Chem. Sci.* **2011**, *2*, 1902.

(8) Peterson, A. A.; Abild-Pedersen, F.; Studt, F.; Rossmeisl, J.; Norskov, J. K. *Energy Environ. Sci.* **2010**, *3*, 1311.

(9) Kuhl, K. P.; Cave, E. R.; Abram, D. N.; Jaramillo, T. F. *Energy Environ. Sci.* **2012**, *5*, 7050.

(10) Hori, Y.; Murata, A.; Takahashi, R.; Suzuki, S. *J. Am. Chem. Soc.* **1987**, *109*, 5022.

(11) Hori, Y.; Murata, A.; Tsukamoto, T.; Wakebe, H.; Koga, O.; Yamazaki, H. *Electrochim. Acta* **1994**, *39*, 2495.

(12) Peterson, A. A.; Nørskov, J. K. *J. Phys. Chem. Lett.* **2012**, *3*, 251.

(13) Kuhl, K. P.; Hatsukade, T.; Cave, E. R.; Abram, D. N.; Kibsgaard, J.; Jaramillo, T. F. *J. Am. Chem. Soc.* **2014**, *136*, 14107.

(14) Gao, F.; Goodman, D. W. *Chem. Soc. Rev.* **2012**, *41*, 8009.

(15) Suo, Y.; Hsing, I. M. *Electrochim. Acta* **2011**, *56*, 2174.

(16) Jirkovský, J. S.; Panas, I.; Romani, S.; Ahlberg, E.; Schiffrin, D. J. *J. Phys. Chem. Lett.* **2012**, 315.

(17) Plana, D.; Florez-Montano, J.; Celorrio, V.; Pastor, E.; Fermin, D. J. *Chem. Commun.* **2013**, *49*, 10962.

(18) Hahn, C.; Abram, D. N.; Hansen, H. A.; Hatsukade, T.; Jackson, A.; Johnson, N. C.; Hellstern, T. R.; Kuhl, K. P.; Cave, E. R.; Feaster, J. T.; Jaramillo, T. F. *J. Mater. Chem. A* **2015**, *3*, 20185.

(19) Kortlever, R.; Balemans, C.; Kwon, Y.; Koper, M. T. M. *Catal. Today* **2015**, *244*, 58.

(20) Sheridan, L. B.; Czerwiniski, J.; Jayaraju, N.; Gebregziabiher, D. K.; Stickney, J. L.; Robinson, D. B.; Soriaga, M. P. *Electrocatal.* **2012**, *3*, 96.

(21) Kwon, Y.; Koper, M. T. M. *Analytical Chemistry* **2010**, *82*, 5420.

(22) Wonders, A. H.; Housmans, T. H. M.; Rosca, V.; Koper, M. T. M. *J. Appl. Electrochem.* **2006**, *36*, 1215.
(23) Kas, R.; Kortlever, R.; Milbrat, A.; Koper, M. T. M.; Mul, G.; Baltrusaitis, J. *Phys. Chem. Chem. Phys.* **2014**, *16*, 12194.
(24) Kas, R.; Kortlever, R.; Yılmaz, H.; Koper, M. T. M.; Mul, G. *ChemElectroChem* **2014**, *3*, 354.
(25) Hoshi, Y. N., M; Suzuki, T.; Hori, Y. *J. Electroanal. Chem.* **1997**, *421*, 15.
(26) Kolbe, D.; Vielstich, W. *Electrochim. Acta* **1996**, *41*, 2457.
(27) Noda H.; Ikeda S.; Yamamoto A.; Einaga H.; K., I. *Bull. Chem. Soc. Jap.* **1995**, *68*, 1889.
(28) Hori, Y.; Wakebe, H.; Tsukamoto, T.; Koga, O. *Electrochim. Acta* **1994**, *39*, 1833.
(29) Chen, Y.; Li, C. W.; Kanan, M. W. *J. Am. Chem. Soc.* **2012**, *134*, 19969.
(30) Grigoriev, S. A.; Millet, P.; Fateev, V. N. *J. Power Sources* **2008**, *177*, 281.
(31) Greeley, J.; Jaramillo, T. F.; Bonde, J.; Chorkendorff, I. B.; Norskov, J. K. *Nat. Mat.* **2006**, *5*, 909.
(32) Ohkawa, K.; Hashimoto, K.; Fujishima, A. *J. Electroanal. Chem.* **1993**, *345*, 445.
(33) Moulder, J. F.; Stickle, W. F.; Sobol, P. E.; Bomben, K. D. in *Handbook of X-ray Photoelectron Spectroscopy*; Physical Electronics, Inc., 1995.
(34) Jenks, C. J.; Chang, S.-L.; Anderegg, J. W.; Thiel, P. A.; Lynch, D. W. *Phys. Rev. B* **1996**, *54*, 6301.
(35) Sreekanth, N.; Pani, K. L. *Chem. Commun.* **2014**, *50*, 11143.
(36) Shibata, H.; Moulijn, J. A.; Mul, G. *Catal. Lett.* **2008**, *123*, 186.
(37) Lee, S.; Kim, D.; Lee, J. *Angew. Chem. Int. Ed.* **2015**, *127*, 1.
(38) Gao, D.; Zhou, H.; Wang, J.; Miao, S.; Yang, F.; Wang, G.; Wang, J.; Bao, X. *J. Am. Chem. Soc.* **2015**, *137*, 4288.
(39) Schouten, K. J. P.; Qin, Z.; Gallent, E. P.; Koper, M. T. M. *J Am Chem Soc* **2012**, *134*, 9864.
(40) Van Der Laan, G. P.; Beenackers, A. A. C. M. *Catalysis Reviews* **1999**, *41*, 255.
(41) Koel, B. E.; Sellidj, A.; Paffett, M. T. *Phys. Rev. B* **1992**, *46*, 7846.